eISSN (Online): 2598-0580

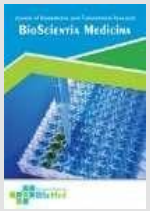

Bioscientia Medicina: Journal of Biomedicine & Translational Research

Journal Homepage: www.bioscmed.com

Unmasking the Primary: The Role of ^{99m}Tc-Sestamibi SPECT/CT in a Case of Carcinoma of Unknown Primary with Suspected Lung Origin

Jessica Ubercaprita[1]*, Endah Indriani Wahyono[1], Mas Adi Sunardi[2], Herry Herman[3], Bethy Suryawathy Hernowo[4], Basuki Hidayat[1]

[1]Department of Nuclear Medicine and Molecular Theranostics, School of Medicine Universitas Padjadjaran/Dr. Hasan Sadikin General Hospital, Bandung, Indonesia

[2]Department of Radiation Oncology, Dr. Hasan Sadikin General Hospital, Bandung, Indonesia

[3]Department of Orthopaedic Surgery, Dr. Hasan Sadikin General Hospital/School of Medicine Universitas Padjadjaran, Bandung, Indonesia

[4]Department of Anatomical Pathology, Dr. Hasan Sadikin General Hospital/School of Medicine Universitas Padjadjaran, Bandung, Indonesia

ARTICLE INFO

Keywords:
^{99m}Tc-sestamibi
Carcinoma of unknown primary
Lung cancer
Nuclear medicine
SPECT/CT

***Corresponding author:**
Jessica Ubercaprita

E-mail address:
jessubercaprita@gmail.com

All authors have reviewed and approved the final version of the manuscript.

https://doi.org/10.37275/bsm.v9i8.1361

A B S T R A C T

Background: Carcinoma of unknown primary (CUP) is a challenging clinical diagnosis, representing histologically confirmed metastatic cancer where the primary tumor site remains unidentified after a standard diagnostic workup. While ^{18}F-FDG PET/CT is recommended by current guidelines, its accessibility is limited in many regions. This report explores the diagnostic utility of Technetium-99m (^{99m}Tc)-Sestamibi Single Photon Emission Computed Tomography/Computed Tomography (SPECT/CT) as a valuable alternative. **Case presentation:** A 67-year-old female presented with musculoskeletal pain. A biopsy of a right ulnar lesion confirmed metastatic carcinoma. Immunohistochemistry (IHC) suggested a possible primary from the lung, breast, or upper gastrointestinal tract. Due to the unavailability of ^{18}F-FDG PET/CT, a ^{99m}Tc-Sestamibi whole-body scan with SPECT/CT was performed. The scan identified a metabolically active, malignant-appearing nodule in segment 6 of the left lung and confirmed widespread skeletal metastases. Although a lung biopsy was not feasible due to limited access, the patient was treated with a lung cancer protocol. This resulted in significant clinical improvement. **Conclusion:** ^{99m}Tc-Sestamibi SPECT/CT served as a critical diagnostic tool in this case of CUP. It successfully identified a suspected pulmonary primary, enabling targeted therapy and leading to a positive clinical outcome. This case highlights the modality's efficacy as a tumor-seeking agent and underscores its essential role in the diagnostic armamentarium for CUP, particularly in resource-limited healthcare settings.

1. Introduction

Cancer of unknown primary (CUP) stands as one of the most perplexing and challenging entities in modern oncology. Defined as a biopsy-proven metastatic malignancy for which the site of origin cannot be established despite a thorough and standardized medical investigation, CUP accounts for a significant portion of cancer diagnoses.[1] Global estimates suggest that CUP constitutes approximately 2-5% of all new cancer cases, making it the fourth most common cause of cancer death in both men and women when considered as a single group. Patients with CUP often present with aggressive, widespread disease at the time of diagnosis, which contributes to

a generally poor prognosis.[2] The median survival for untreated patients is a mere three to four months, and even with empiric chemotherapy, median survival rates have historically struggled to surpass one year.

The diagnostic algorithm for CUP is a process of exclusion. It begins with a comprehensive patient history and physical examination, followed by routine blood work, serum tumor markers, and initial imaging studies such as chest X-rays and computed tomography (CT) scans of the chest, abdomen, and pelvis.[3] The cornerstone of the diagnosis is the histopathological analysis of a metastatic lesion biopsy. Immunohistochemistry (IHC) plays a pivotal role in this process, utilizing a panel of antibodies to detect specific proteins within tumor cells, thereby narrowing the list of potential primary sites.[4] CUP is histologically diverse, with adenocarcinomas being the most common subtype (approximately 50%), followed by poorly differentiated carcinomas (30%), squamous cell carcinomas (15%), and other undifferentiated neoplasms (5%). The IHC profile can often suggest a likely tissue of origin; for instance, a CK7-positive/CK20-negative profile is commonly associated with tumors of the lung, breast, and upper gastrointestinal tract, among others.

Despite these advanced pathological techniques, the primary tumor remains elusive in a substantial number of cases. This diagnostic ambiguity poses a profound therapeutic dilemma. Modern oncology is increasingly defined by precision medicine, where treatment strategies are tailored to the specific primary tumor type and its unique molecular characteristics.[5] Without knowledge of the primary site, clinicians are often forced to rely on broad-spectrum, empiric chemotherapy regimens that may offer limited efficacy and significant toxicity. Identifying the primary tumor is, therefore, of paramount importance, as it can unlock access to more effective site-specific therapies, targeted agents, immunotherapies, and enrollment in specialized clinical trials, all of which can have a beneficial impact on patient survival and quality of life.

In this context, advanced molecular and functional imaging has emerged as a critical tool. The European Society for Medical Oncology (ESMO) and other international bodies currently recommend Positron Emission Tomography/Computed Tomography with ^{18}F-fluorodeoxyglucose (^{18}F-FDG PET/CT) as the standard of care for identifying the primary tumor in patients with CUP.[6] ^{18}F-FDG, a glucose analog, is taken up by metabolically active cells, allowing for whole-body visualization of tumors, which typically exhibit high glucose metabolism. Numerous studies and meta-analyses have confirmed the high diagnostic yield of ^{18}F-FDG PET/CT, with a reported success rate in identifying the primary tumor in 25-50% of cases, often leading to a change in patient management. However, the clinical utility of ^{18}F-FDG PET/CT is severely hampered by practical constraints, particularly in developing countries and resource-limited regions. The high cost of the scanner, the logistical complexity of producing and distributing the short-lived ^{18}F-FDG radiotracer, and the lack of necessary infrastructure and trained personnel create significant barriers to access.

This gap in accessibility necessitates the exploration and validation of alternative imaging modalities that are more readily available and cost-effective. One such modality is scintigraphy using Technetium-99m (^{99m}Tc)-Sestamibi. ^{99m}Tc-Sestamibi is a lipophilic, cationic radiopharmaceutical that was initially developed for myocardial perfusion imaging. Its mechanism of accumulation is related to cellular and mitochondrial membrane potentials; it passively diffuses into cells and becomes sequestered within the mitochondria of cells with high metabolic activity, a characteristic feature of many malignant tumors.[7] This tumor-seeking property has been successfully exploited for imaging various cancers, including those of the breast, thyroid, parathyroid, and lung. When combined with Single Photon Emission Computed Tomography (SPECT), which provides three-dimensional functional information, and integrated with a low-dose CT for anatomical localization (SPECT/CT), ^{99m}Tc-Sestamibi imaging becomes a

powerful tool for tumor detection and characterization. The fusion of functional and anatomical data provided by SPECT/CT enhances diagnostic accuracy by allowing for precise localization of abnormal radiotracer uptake, distinguishing it from physiologic activity and improving the characterization of lesions.[8] Given that ^{99m}Tc is produced from a generator system, it is far more accessible and affordable than cyclotron-produced PET tracers, making Sestamibi SPECT/CT a feasible imaging option in a greater number of nuclear medicine centers worldwide.[9] While several studies have documented its utility in specific cancers, its role in the complex diagnostic pathway of CUP is less defined, particularly in the modern era of medicine.

The novelty of this case report lies in its detailed illustration of the pivotal role of ^{99m}Tc-Sestamibi SPECT/CT in resolving a classic CUP dilemma in a resource-constrained setting. While ^{18}F-FDG PET/CT remains the guideline-recommended modality, this case demonstrates that Sestamibi SPECT/CT is not merely a suboptimal alternative but a robust and effective diagnostic tool capable of identifying a suspected primary tumor with sufficient confidence to guide definitive, site-specific therapy and achieve a positive clinical outcome.[10] The aim of this study is to present comprehensive clinical and imaging evidence from a patient with CUP, showcasing how ^{99m}Tc-Sestamibi SPECT/CT successfully identified a putative pulmonary primary and multiple metastatic sites, directly influenced the therapeutic strategy, and highlights the modality's significant clinical utility in the management of this challenging oncologic entity.

2. Case Presentation

In March 2023, a 67-year-old Indonesian female presented to the Orthopedic Department of Dr. Hasan Sadikin General Hospital with a two-month history of progressively worsening, persistent pain. The pain was localized to the right elbow, with radiation down to the lower arm, and was also present in both knees. The pain intensified with physical activity. Her medical history was non-contributory; she had no personal history of hypertension, diabetes mellitus, asthma, or known allergies, and she explicitly denied any family history of malignancy. For symptomatic relief, she had been self-medicating with mefenamic acid three times daily since the onset of her symptoms. Upon physical examination, the patient appeared to be in moderate distress due to pain but was fully conscious and alert (compos mentis). Her vital signs were stable: blood pressure was 130/80 mmHg, pulse rate was 84 beats per minute and regular, respiratory rate was 16 breaths per minute, and her body temperature was 36.6°C. Examination of the extremities revealed visible swelling of the right elbow, right lower arm, and both knees. Palpation of these areas elicited significant tenderness. The patient rated her pain as a 4 on a 10-point numeric rating scale. A detailed summary of the patient's initial presentation and diagnostic findings is presented in Table 1.

Table 1. Summary of patient's clinical findings at presentation.

Parameter	Details
Demographics	67-year-old female, Indonesian
Chief complaints	Progressive pain in the right elbow radiating to the lower arm and both knees for 2 months.
History of illness	No personal history of major chronic diseases or malignancy. No family history of malignancy.
Physical examination	**Vitals:** BP 130/80 mmHg, HR 84/min, RR 16/min, Temp 36.6°C. **Extremities:** Swelling and tenderness on palpation of the right elbow and both knees. **Pain Score:** 4 out of 10 on the numeric rating scale.
Laboratory findings	**Tumor Markers (31/03/2023):**- CEA: 37.09 ng/mL (Normal: ≤5.0) - CA-125: 637.3 U/mL (Normal: ≤35.0). **CBC:** Mild normocytic anemia (Hb: 10.8 g/dL). **CMP:** Elevated Alkaline Phosphatase (350 U/L).
Initial imaging	**Chest X-Ray (10/04/2023):** Suspicious for intrapulmonary metastasis. **Bone Survey (02/05/2023):** Suspected metastatic disease in the calvaria, right ulna, bilateral tibia, and left fibula.
Histopathology	**Right Ulna Biopsy (13/04/2023):** Confirmed metastatic carcinoma.
Immunohistochemistry	**Profile:** CK7 Positive, CK20 Negative, PAX8 Negative. **Interpretation:** Suggested primary origin from the lung, breast, mesothelium, gaster, pancreas, or salivary glands.

Initial laboratory investigations revealed markedly elevated serum tumor markers: Carcinoembryonic Antigen (CEA) was 37.09 ng/mL and Cancer Antigen 125 (CA-125) was 637.3 U/mL. A complete blood count (CBC) showed mild normocytic anemia, and a comprehensive metabolic panel (CMP) was notable for elevated alkaline phosphatase, suggestive of bone metastatic activity. A chest X-ray was suspicious for intrapulmonary metastasis. Given the patient's severe, localized bone pain, a biopsy of the right ulna was performed and confirmed the presence of metastatic carcinoma, establishing the diagnosis of Carcinoma of Unknown Primary. A subsequent skeletal bone survey revealed multiple lytic lesions suspicious for metastases in several bones. Following these findings, the patient was referred to the Department of Nuclear Medicine and Molecular Theranostics for a whole-body scan to attempt to localize the primary tumor.

Due to the unavailability of ^{18}F-FDG PET/CT at the institution and its high associated costs, a ^{99m}Tc-Sestamibi whole-body scan (WBS) with SPECT/CT was selected as the primary imaging modality for this purpose. The patient provided informed consent after the procedure, potential risks, and benefits were explained. She was instructed to have a light, fatty meal after radiotracer injection to promote hepatobiliary clearance and improve image quality in the abdomen. An intravenous line was placed, and the patient was injected with a dose of 740 MBq (20 mCi) of ^{99m}Tc-Sestamibi. Planar whole-body images were acquired at 15 minutes (early phase) and 120 minutes (delayed phase) post-injection. The scans were performed on a dual-head SPECT/CT system equipped with low-energy, high-resolution (LEHR) collimators. Following the delayed planar imaging, SPECT/CT was performed over the chest and any other regions demonstrating suspicious uptake. For the SPECT acquisition, a 128x128 matrix was used with 64 projections over a 360-degree rotation. The subsequent low-dose CT scan was performed for attenuation correction and anatomical localization using a 512x512 matrix and 3mm slice thickness. The early and delayed planar images both demonstrated multiple focal areas of intense, persistent radiotracer uptake in the skeleton. These were clearly visualized in the right ulna, bilateral tibiae, and the left cuneiform bone, as indicated by the red arrows in Figure 1. The persistence of uptake on delayed imaging was highly suggestive of malignant involvement rather than inflammatory change. The SPECT/CT images confirmed the findings from the planar scan and identified additional metastatic sites with greater anatomical precision (Figure 2). Fused SPECT/CT images revealed metabolically active lesions corresponding to lytic changes on CT in the occipital bone (Figure 2A), the right ulna (Figure 2B), the left acetabulum (Figure 2C), the right tibia (Figure 2D), the left fibula (Figure 2E), and the left medial cuneiform bone (Figure 2F). The combination of functional and anatomical data provided by SPECT/CT allowed for definitive characterization of these sites as skeletal metastases. This was the most critical part of the examination. The SPECT/CT of the chest identified a solitary, intensely avid nodule in segment 6 (the superior segment of the lower lobe) of the left lung (Figure 3). The fused images showed a clear focal area of high radiotracer uptake corresponding to a soft-tissue pulmonary nodule on the CT component. The pattern of intense and focal uptake was highly suspicious for a primary lung malignancy. A semi-quantitative analysis was performed, yielding a tumor-to-contralateral background ratio of 4.5, further strengthening the suspicion of malignancy. The scan also noted several non-avid findings of lesser importance, including fibrotic lesions and multiple subcentimeter calcified nodules in the upper lobes of both lungs, likely representing post-inflammatory or post-infectious scarring. A simple left renal cyst and cholelithiasis (gallstones) were also incidentally identified on the CT portion of the scan.

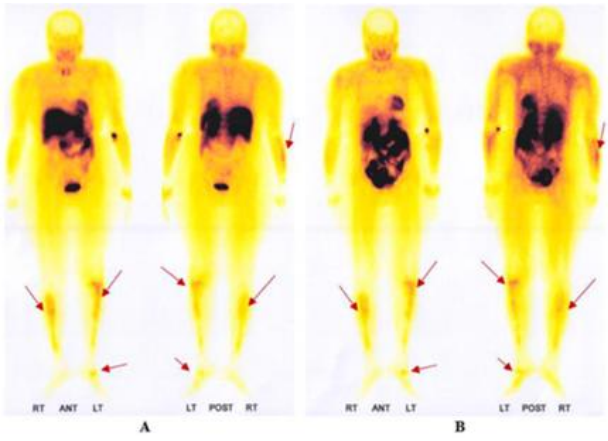

Figure 1. Whole-body scintigraphy using ^{99m}Tc-Sestamibi. (A) Early image at 15 minutes post-injection demonstrates increased ^{99m}-Tc radiotracer uptake in the right ulna, bilateral tibiae, and left cuneiform bone (red arrows). (B) Delayed image at 120 minutes post-injection confirms persistent uptake in the same regions (red arrows).

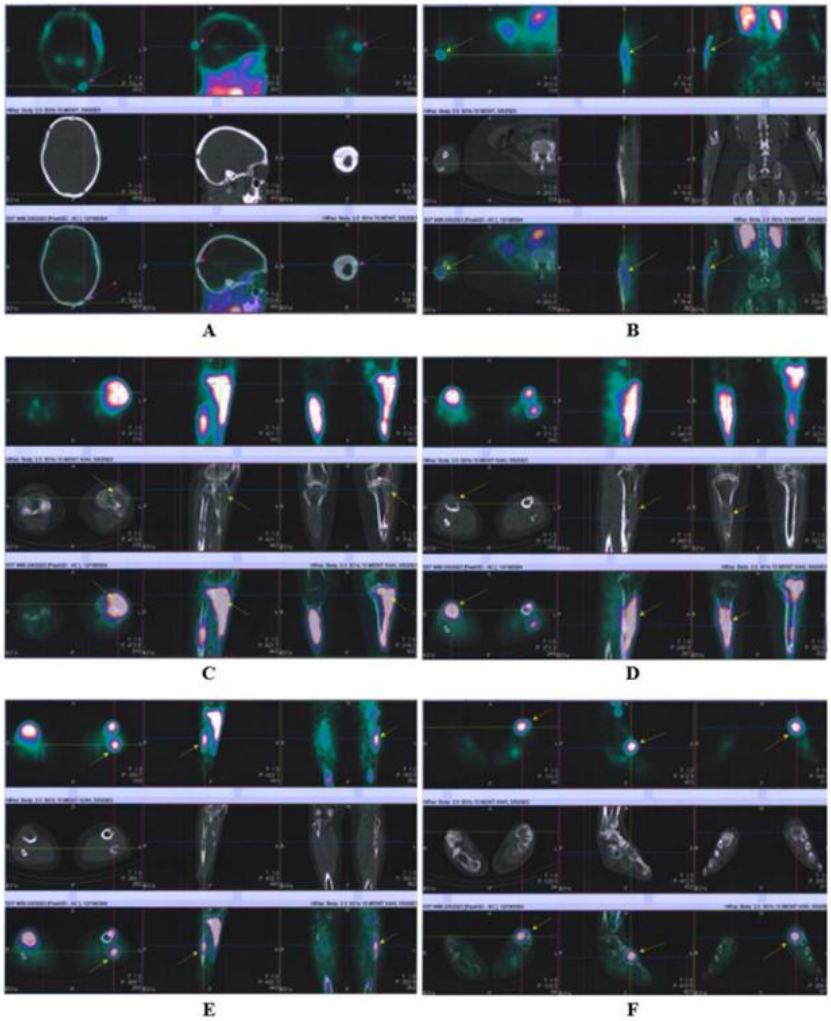

Figure 2. SPECT/CT imaging demonstrates persistent radiopharmaceutical uptake in multiple skeletal regions, consistent with metastatic involvement. (A–F) Axial, coronal, and sagittal fused SPECT/CT images show increased uptake in previously identified areas (right ulna, bilateral tibiae, and left cuneiform). Additional sites of abnormal tracer accumulation include the occipital bone (A), the right ulna (B), left acetabulum (C), right tibiae (D), left fibula (E), and left medial cuneiform bone (F), all of which are suspicious for skeletal metastases. The combination of functional and anatomical imaging provides accurate localization of metabolically active lesions.

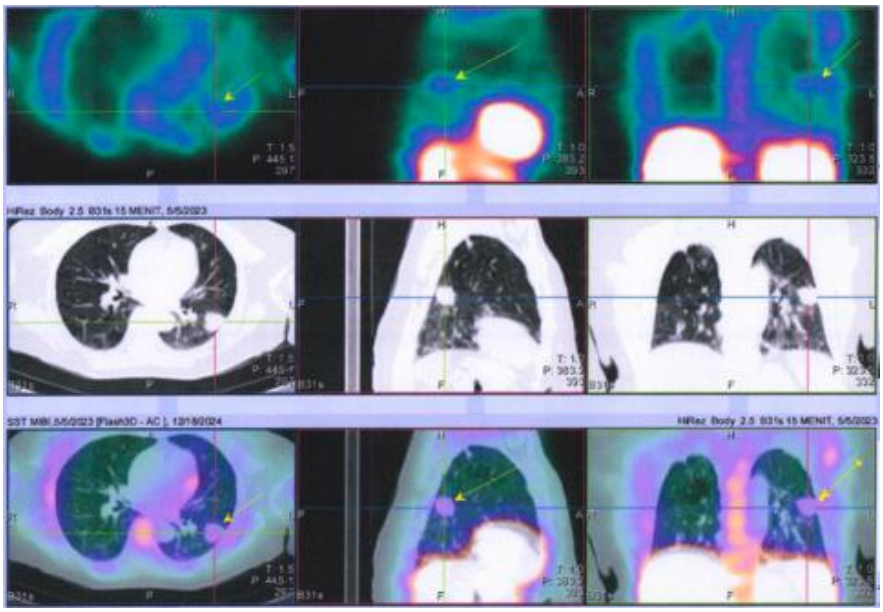

Figure 3. SPECT/CT imaging of the thoracic region. Fused axial, sagittal, and coronal SPECT/CT images demonstrate a focal area of increased radiotracer uptake in segment 6 of the left lung lobe (yellow arrows), corresponding to a hypermetabolic pulmonary nodule. The pattern of uptake and anatomical localization is suspicious for a malignant lesion.

Following the ^{99m}Tc-Sestamibi SPECT/CT scan, a review of the initial biopsy from the right ulna was undertaken with a specific request for immunohistochemistry (IHC). The IHC panel showed that the tumor cells were positive for Cytokeratin 7 (CK7) and negative for both Cytokeratin 20 (CK20) and Paired box gene 8 (PAX8). This profile strongly corroborated the imaging findings that pointed towards the lung as the primary site. A biopsy of the suspicious lung nodule was recommended for definitive histopathological confirmation but was deemed not feasible due to limited accessibility. Given the compelling convergent evidence from the clinical presentation, tumor markers, IHC profile, and the definitive ^{99m}Tc-Sestamibi SPECT/CT findings, a multidisciplinary tumor board reached a consensus diagnosis of a presumed primary lung carcinoma with widespread skeletal metastases. Based on this diagnosis, the patient was initiated on a standard treatment protocol for metastatic non-small cell lung cancer. This treatment plan and the subsequent outcomes are detailed in Table 2.

Table 2. Summary of patient's treatment and follow-up.

Parameter	Details
Consensus diagnosis	Presumed primary lung carcinoma with multiple skeletal metastases.
Treatment rationale	Based on convergent evidence from IHC (CK7+/CK20-/PAX8-) and Sestamibi SPECT/CT findings (avid lung nodule) pointing to a pulmonary origin.
Systemic therapy	**Chemotherapy:** Paclitaxel-Carboplatin doublet regimen, a standard of care for metastatic non-small cell lung cancer. **Bone-Targeted Therapy:** Zoledronic Acid (4 mg), a bisphosphonate to manage skeletal-related events.
Radiotherapy	**Technique:** External Beam Radiotherapy (EBRT). **Target:** Palliative intent to the chest region, targeting the presumed primary lung tumor. **Dose & Fractionation:** 10 sessions.
Follow-up	Evaluation conducted two months after initiation of therapy.
Clinical outcome	**Result:** Significant clinical improvement was observed. **Specifics:**- Marked reduction in pain in the right arm and both knees.- Decreased requirement for analgesic medication.- Resolution of swelling in the extremities.

The patient tolerated the treatment well. A follow-up evaluation conducted two months after the initiation of therapy showed significant clinical improvement. She reported a marked reduction in pain in her right arm and knees, with a decreased need for analgesic medication. The swelling in her extremities had also subsided. This positive therapeutic response further substantiated the accuracy of the presumed diagnosis of a pulmonary primary.

3. Discussion

The clinical journey of a patient diagnosed with carcinoma of unknown primary (CUP) is one fraught with uncertainty, a diagnostic odyssey that challenges the very foundations of modern, site-specific oncology.[10] The case presented here, that of a 67-year-old woman with biopsy-proven metastatic carcinoma in her ulna but no identifiable primary source, epitomized this classic and formidable clinical dilemma. The successful navigation of this case, moving from a state of profound ambiguity to a confident, actionable diagnosis and a positive therapeutic outcome, serves as a powerful testament to the synergy between astute pathological analysis and advanced, accessible functional imaging. The pivotal role was played by Technetium-99m (^{99m}Tc)-Sestamibi Single Photon Emission Computed Tomography/Computed Tomography (SPECT/CT), a modality that, in this instance, stepped beyond its conventional applications to illuminate a path forward where the standard-of-care imaging was unavailable.[11] This discussion will embark on a detailed exploration of this case, deconstructing the significance of the immunohistochemical findings, delving into the intricate pathophysiology that allows Sestamibi to act as a metabolic spy, celebrating the indispensable power of hybrid imaging, and ultimately, weaving these threads together to underscore the profound clinical impact of achieving a presumptive diagnosis in the challenging landscape of CUP.

The diagnosis of CUP lands as a heavy blow, not only for the patient who must grapple with having a cancer whose origin is a mystery, but also for the clinician who is deprived of the most fundamental piece of information needed to guide treatment. This entity, sometimes referred to as an "orphan" tumor, is defined by its metastatic presentation in the absence of a detectable primary tumor despite a standardized and thorough investigation. It is not a rare curiosity; CUP accounts for a significant portion of all cancer diagnoses, with global estimates placing its incidence at approximately 3-5% of all malignancies. This position CUP as one of the ten most frequent cancer presentations worldwide. The aggressive biology often associated with CUP means that patients frequently presented with widespread disease at diagnosis, contributing to a historically grim prognosis.[12] This case was no exception, with the patient presenting with multiple painful skeletal lesions, a hallmark of advanced disease.

The histopathological heterogeneity of CUP adds another layer of complexity. As noted in the literature, the majority of CUP cases were adenocarcinomas (approximately 50%), followed by poorly differentiated carcinomas or undifferentiated neoplasms (30%), and squamous cell carcinomas (15%).[11] The initial biopsy from this patient's right ulna confirmed a metastatic carcinoma, placing her within this broad and challenging group. Autopsy studies, long considered the ground truth in identifying the elusive primary sites in CUP, have consistently shown that the most common occult primaries were tumors of the lung and pancreas. This historical data provided a crucial context for this case, suggesting from the outset that a careful search within the thorax and abdomen was warranted. The patient’s clinical presentation, with widespread bone metastases from an adenocarcinoma, fit into one of the "unfavorable" subsets of CUP, a category typically associated with a median survival of less than a year even with treatment. This stark prognosis underscored the critical importance and urgency of the diagnostic quest. The goal was not merely academic; identifying

the primary tumor held the potential to shift the patient from a generic, empiric treatment protocol to a more effective, evidence-based, site-specific therapy that could alter her clinical course. The entire diagnostic process was therefore a race against time, a systematic effort to unmask the tumor's identity before its relentless progression could overwhelm the patient.

In the labyrinth of CUP, immunohistochemistry (IHC) serves as the master key, a technique that translates the static morphology of a tumor cell into a dynamic expression of its lineage.[13] The IHC panel performed on the ulnar metastasis in this patient yielded a precise molecular signature: CK7-positive, CK20-negative, and PAX8-negative. This was the first major breakthrough in the case, a series of molecular clues that systematically narrowed the vast landscape of potential primary tumors into a manageable and highly probable list of suspects. The foundation of this panel rested on the differential expression of cytokeratins (CKs), which were intermediate filament proteins forming the structural backbone of epithelial cells. Their expression patterns were highly conserved and tissue-specific, making them exceptional markers of cellular origin. Cytokeratin 7 (CK7) was a high-molecular-weight cytokeratin whose expression was typically found in the epithelial cells of the lung, breast, female genital tract (ovary, endometrium), biliary system, pancreas, and salivary glands. Its strong and diffuse positivity in the metastatic tumor cells was a powerful initial finding. It immediately oriented the diagnostic search towards these specific organ systems. Lung adenocarcinomas, for example, express CK7 in over 90% of cases, making it a highly sensitive marker for a pulmonary primary. Similarly, the majority of breast carcinomas were also CK7-positive. Thus, the CK7 result alone placed lung and breast cancer high on the differential diagnosis.

The second part of this classic IHC duo, Cytokeratin 20 (CK20), provided equally important, albeit negative, information. In stark contrast to the broad expression of CK7, CK20 had a very restricted pattern of expression, found almost exclusively in the glandular cells of the gastrointestinal tract, particularly the colorectum, and in the specialized urothelial cells lining the bladder and urinary tract.[14] Its utility, therefore, was primarily as a marker for colorectal adenocarcinoma and urothelial carcinoma. The definitive lack of CK20 expression in this patient's tumor cells was a powerful piece of exclusionary evidence. It made a primary colorectal cancer, one of the most common malignancies worldwide and a frequent cause of metastases, extremely unlikely. The resulting CK7+/CK20- immunophenotype was a classic signature. This profile is the single most common pattern found in adenocarcinomas of the lung (over 90%), breast (over 90%), and ovary (around 80-90%), while being exceptionally rare in colorectal cancer (less than 5%). This single pair of markers had, with remarkable efficiency, filtered out a major contender and amplified the signal pointing towards a thoracic or breast origin.

The final piece of this molecular puzzle, PAX8, delivered another critical layer of diagnostic exclusion. PAX8, or Paired box gene 8, was not a structural protein like the cytokeratins, but a transcription factor essential for the embryonic development of the kidney, thyroid gland, and the female reproductive organs of Müllerian origin (fallopian tubes, uterus, and ovaries).[9] Critically, the expression of PAX8 was retained in the vast majority of carcinomas arising from these specific tissues. It was therefore considered a highly specific and reliable lineage marker for renal cell carcinoma, papillary and follicular thyroid carcinoma, and high-grade serous carcinomas of the ovary. The negative staining for PAX8 in the metastatic cells was profoundly informative. It effectively ruled out a renal primary and made a thyroid origin exceptionally improbable. Furthermore, it significantly lowered the probability of an ovarian primary, despite the patient’s markedly elevated CA-125 level (a tumor marker that, while classic for ovarian cancer, is notoriously non-specific and can be elevated in many conditions, including lung cancer, pancreatitis, and even benign inflammatory states).

In synthesizing these three distinct IHC results, the diagnostic picture sharpened dramatically. The positive CK7 result created a list of possibilities. The negative CK20 and PAX8 results then acted as erasers, systematically removing major organ systems from that list. What remained after this process of molecular deduction was a short, high-probability list of candidate primaries, with lung adenocarcinoma and breast carcinoma as the undisputed frontrunners. The IHC report, which explicitly suggested origins including the lung, breast, or pancreas, had fulfilled its purpose perfectly.[10] It had transformed the case from a complete unknown into a focused clinical problem with a clear direction for the subsequent imaging investigation.

Guided by the molecular signposts of the IHC panel, the clinical team required an imaging modality capable of surveying the entire body to locate the hidden primary tumor. The selection of ^{99m}Tc-Sestamibi SPECT/CT was a decision rooted in a deep understanding of the unique pathophysiology of both the radiopharmaceutical and the cancer cell itself.[15] Sestamibi was not merely a passive dye; it was an active metabolic spy, designed to exploit the fundamental bioenergetic alterations that define malignancy.

The journey of a Sestamibi molecule from the bloodstream into a cancer cell was a tale of charge and potential. The molecule itself was a complex of Technetium-99m, a gamma-emitting radioisotope, chelated within an organic structure that rendered it lipophilic (fat-soluble) and imparted a net positive electrical charge (a cation).[16] Its lipophilicity allowed it to effortlessly diffuse through the fatty lipid bilayer that constitutes the cell membrane, a critical first step for entry. The driving force for this entry was the cell's own transmembrane electrical potential. All cells maintain a negative charge on the inside relative to the outside, but this electrochemical gradient was often significantly increased in cancer cells due to alterations in ion pump and channel activity. This heightened negative interior acted as an electrical beacon, actively pulling the positively charged Sestamibi molecules out of the circulation and into the cell's cytoplasm.

However, simple entry into the cytoplasm was not enough to create a high-quality image. The true genius of Sestamibi's design laid in its subsequent sequestration within the mitochondria. Mitochondria were the powerhouses of the cell, and to perform their function of generating ATP, they maintained an even more profoundly negative electrical potential across their inner membrane, typically ranging from -150mV to -180mV.[13] This was, by far, the most negative electrochemical compartment within the entire cell. This intense negative charge created an irresistible electrical sink for the Sestamibi molecules that had entered the cytoplasm. They were drawn into the mitochondria and effectively trapped there, accumulating to very high concentrations. This mitochondrial trapping was the key to Sestamibi's high tumor-to-background ratio and its ability to visualize tumors with high clarity.

This entire mechanism was intimately linked to the unique metabolic state of cancer cells. Many tumors, including the majority of non-small cell lung cancers, were characterized by a state of heightened metabolic activity and a large mitochondrial mass to fuel their relentless growth and proliferation. They were, in essence, cellular engines running in overdrive. By targeting the mitochondria, Sestamibi was directly imaging this core feature of malignancy. It was a functional map of the cancer's energy infrastructure.[14] This property had long been exploited in oncology, and its use in this CUP case was a logical extension of its well-documented tumor-seeking capabilities in breast, lung, and thyroid malignancies. The decision to use Sestamibi was therefore not a shot in the dark, but a calculated application of a metabolic probe designed to seek out and flag the very machinery that made cancer cells so dangerous.

While the Sestamibi molecule provided the signal, the SPECT/CT scanner provided the clarity and context necessary to interpret that signal correctly. Using traditional, two-dimensional planar scintigraphy alone would have been a profoundly

limited approach.[15] The planar whole-body images acquired in this case (Figure 1) were invaluable as a first look, a "scout map" of the disease. They efficiently surveyed the entire body from head to toe, clearly demonstrating the widespread nature of the skeletal disease by revealing multiple "hot spots" of intense, persistent radiotracer uptake in the right ulna, both tibiae, and the left cuneiform bone. This persistence on delayed imaging was a key feature, suggesting malignant metabolic activity rather than transient inflammatory uptake. However, a planar image was an imperfect map; it was a shadowgram, collapsing a three-dimensional body into a two-dimensional picture. This process created significant problems with overlying and underlying structures, which could obscure or mimic disease. A hot spot in the chest, for instance, could be in the lung, the rib, the heart, or the liver, and a planar image could not reliably differentiate among them.

This was where the transformative power of hybrid imaging came into play. The first step up from planar imaging was Single Photon Emission Computed Tomography (SPECT).[16] By rotating the gamma cameras around the patient, SPECT acquired data from multiple angles, which a powerful computer then used to reconstruct a true three-dimensional image of the radiotracer's distribution. This 3D dataset, which could be viewed in axial, coronal, and sagittal slices, already provided a massive improvement in diagnostic information, allowing for much better separation of adjacent structures and localization of abnormalities. The true revolution, however, was the integration of a low-dose Computed Tomography (CT) scanner into the same machine. Acquiring a CT scan in the same session, with the patient in the same position, provided a high-resolution anatomical roadmap. The magic happened when the functional SPECT data and the anatomical CT data were digitally fused together. This fusion of form and function was the core strength of SPECT/CT, and its value in this case cannot be overstated.

The SPECT/CT images of the thorax (Figure 3) provided the single most important finding of the entire diagnostic workup. The CT component identified a discrete, soft-tissue nodule measuring approximately 1.5 cm, located anatomically in the superior segment (segment 6) of the left lower lobe. The SPECT component showed that this precise anatomical structure was the source of intense, focal, and avid radiotracer accumulation. The fused image left no room for doubt. It was not physiologic uptake in the heart, which was seen separately. It was not activity in a rib. It was, with very high certainty, a metabolically active and therefore highly suspicious malignant lesion within the lung parenchyma. This act of fusion transformed a non-specific finding into a definitive and actionable one.

The same principle applied to the evaluation of the skeletal disease (Figure 2). The SPECT/CT images of the skeleton took the hot spots seen on the planar scan and gave them precise anatomical correlates. The uptake in the right ulna was shown to correspond to a destructive lytic lesion. Additional sites of disease, such as in the occipital bone and the left acetabulum, were identified with a clarity that the planar scan could not provide. This confirmed that the lesions were not only metabolically active but also associated with structural bone damage, solidifying their characterization as metastases. By providing this exquisite level of detail, the SPECT/CT scan not only located the probable primary tumor but also provided a more accurate and comprehensive staging of the patient’s metastatic disease, all in a single imaging session.

The diagnostic journey in this case reached its climax not with a single test result, but with the powerful convergence of two independent and robust lines of evidence. It was a masterful demonstration of the multidisciplinary approach that defines modern cancer care. The first pillar of evidence was molecular, provided by the pathologists. The CK7+/CK20-/PAX8- immunophenotype was a clear and compelling molecular signature that pointed squarely towards a primary tumor of either lung or breast origin. The second pillar was functional and anatomical, provided by the nuclear medicine physicians and radiologists.

The ^{99m}Tc-Sestamibi SPECT/CT scan had identified a solitary, hypermetabolic nodule in the left lung that had all the characteristics of a primary malignancy, along with providing a detailed map of the extensive skeletal metastases.[17]

When these two pillars of evidence were placed side-by-side, they aligned perfectly. They converged upon a single, unified, and overwhelmingly probable diagnosis: this patient was suffering from a primary lung adenocarcinoma that had metastasized to her bones. The alternative possibilities became vanishingly small. The likelihood that this patient had, for example, an occult breast cancer primary AND a completely unrelated, incidental lung nodule that also happened to be intensely Sestamibi-avid was clinically improbable to the point of being discountable. The simplest explanation—that the avid lung nodule was the primary source of the CK7-positive metastasis—was by far the most logical and compelling.[18]

This high degree of diagnostic certainty, achieved even in the absence of a direct biopsy of the lung lesion, was what empowered the clinical oncology team to act decisively. They were able to move beyond the therapeutic paralysis that often accompanies a CUP diagnosis. Instead of resorting to a non-specific, "best guess" empiric chemotherapy regimen, they could confidently initiate a targeted, guideline-directed treatment protocol specifically for metastatic non-small cell lung cancer. The selected regimen of paclitaxel-carboplatin was a standard of care for this diagnosis, and the addition of zoledronic acid was the appropriate management for her extensive bone disease. Furthermore, the precise localization of the primary lesion in the lung allowed the radiation oncology team to plan and deliver palliative radiotherapy directly to the source of the cancer, an option that would not have been possible without the SPECT/CT findings.[19]

The final, and perhaps most scientifically satisfying, piece of evidence in this entire case was the patient's own clinical response. Her significant clinical improvement—the reduction in her debilitating pain and swelling—following the initiation of this targeted therapy was more than just a positive outcome; it was the ultimate retrospective validation of the diagnostic process. This positive therapeutic response, an argument ex juvantibus (from that which helps), served as the final confirmation that the diagnosis was correct. It affirmed that the multidisciplinary team had successfully identified the enemy's headquarters and that the targeted therapeutic strike had been effective. This transformed the presumptive diagnosis into a functionally certain one, bringing the patient's arduous diagnostic odyssey to a successful and hopeful conclusion. This case, therefore, was not merely about an interesting set of images; it was about a meticulous, logical, and ultimately successful diagnostic process that serves as a blueprint for tackling this most challenging of oncologic puzzles, particularly in settings where physicians must make the most of what is available to them.[20]

4. Conclusion

This case of carcinoma of unknown primary (CUP) powerfully demonstrates the diagnostic capability of ^{99m}Tc-Sestamibi SPECT/CT in unmasking a hidden malignancy. In a clinical scenario complicated by the unavailability of 18F-FDG PET/CT, this accessible imaging modality successfully identified a solitary hypermetabolic pulmonary nodule, pinpointing the suspected primary tumor with high confidence. When interpreted in synergy with immunohistochemical findings, the scan provided a sufficiently confident diagnosis to guide definitive, site-specific therapy. The patient's subsequent clinical improvement following lung cancer-directed treatment served as the ultimate validation of the diagnostic accuracy. This report underscores that ^{99m}Tc-Sestamibi SPECT/CT is a robust, effective, and essential tool in the diagnostic armamentarium for CUP. It offers a critical pathway to diagnostic clarity and informed therapeutic decision-making, potentially improving patient outcomes, particularly in resource-limited healthcare settings where PET/CT is not readily available.

5. References

1. Fang S, Zhu Q-L, Liu Y-M, Zhang Z-H, Wang O, Xing X-P, et al. Localization of ectopic hyperparathyroidism: Ultrasound versus ^{99m}Tc-sestamibi, 4-dimensional computed tomography, and 11C-choline positron emission tomography/computed tomography. Endocr Pract. 2024; 30(3): 239–45.
2. Mansour S, Alanazi A, Alshammari A, Almutairi F, Dalilah J, Hakami R, et al. Diagnostic Performance of 18F-fluorocholine PET/CT Compared to ^{99m}Tc-Sestamibi Scintigraphy in Diagnosis of Parathyroid Adenoma. Int J Biomed. 2024; 14(1): 83–7.
3. Mandic A, Kraljevic I, Skoric Polovina T, Zibar Tomsic K, Dusek T, Balasko A, et al. Diagnostic performance of ^{99m}Tc-sestamibi SPECT/CT and 18F-choline PET/CT in locating hyperfunctioning parathyroid glands in patients with primary hyperparathyroidism. Exp Clin Endocrinol Diabetes. 2024; 132(4): 216–20.
4. Fiore R, Gombert E, La Rosa S, Dunet V, Sykiotis GP, Gorostidi F. Esophageal schwannoma mimicking non-functional parathyroid adenoma on ^{99m}Tc-sestamibi imaging: a case report. Front Endocrinol (Lausanne). 2024; 15: 1258233.
5. Mandic A, Kraljevic I, Skoric PT, Zibar TK, Dusek T, Balasko A, et al. The usefulness of 18F-choline PET/CT in patients with negative findings on ^{99m}Tc-sestamibi SPECT/CT in Locating Hyperfunctioning Parathyroid Glands in Primary Hyperparathyroidism. Endocr Abstr. 2024.
6. Gürlüler E. Diagnostic performance of ultrasound versus ^{99m}Tc-sestamibi scintigraphy in preoperative depiction and localization of parathyroid adenoma in patients with primary hyperparathyroidism. Eur Res J. 2025; 11(1): 88–97.
7. Jarvis P, Dixon K, O'Shaughnessy E, Downs J, Richardson T, Parekh A. Improving parathyroid localisation in the ^{99m}Tc-sestamibi scan. Clin Radiol. 2025; 83(106883): 106883.
8. Dropmann JA, Kleespies A, Fuerst H, Kremer M, Drefs M, Neuberger M. Importance of oxyphil cells for ^{99m}Tc-sestamibi uptake in primary hyperparathyroidism: a retrospective observational study. Nuklearmedizin. 2025; 64(3): 215–24.
9. Fernando PEA, Bautista PA. Utility of ^{99m}Tc-sestamibi SPECT/CT in the early localization of metastatic parathyroid carcinoma. Asia Ocean J Nucl Med Biol. 2018; 6(2): 171–8.
10. Singh H, Wale DJ, Wong KK, Gross MD, Viglianti BL. Synchronous metastatic breast carcinoma and parathyroid adenoma on 18F-FDG PET/CT and ^{99m}Tc-sestamibi imaging. Clin Nucl Med. 2019; 44(2): 148–9.
11. Cadena-Piñeros E, De Los Reyes CA, Llamas-Olier A, Romero-Rojas AE. Advantages of the ^{99m}Tc-sestamibi single-photon emission computed tomography/computed tomography in occult parathyroid adenoma and concomitant thyroid papillary carcinoma. Indian J Nucl Med. 2019; 34(2): 150–2.
12. Zhang M, Sun L, Rui W, Guo R, He H, Miao Y, et al. Semi-quantitative analysis of ^{99m}Tc-sestamibi retention level for preoperative differential diagnosis of parathyroid carcinoma. Quant Imaging Med Surg. 2019; 9(8): 1394–401.
13. Malipedda S, Kamaleshwaran KK, Muthusamy D, Veerasamy M, Soundararajan AP, Jayaraj AV. Rare imaging findings of concomitant presence of multiple parathyroid adenomas and carcinoma in a chronic kidney disease patient with tertiary hyperparathyroidism detected on ^{99m}Tc-Sestamibi single-photon-emission computed tomography/computed tomography scintigraphy. Indian J Nucl Med. 2020; 35(4): 333–5.

14. Wang W, Liu J, Liu J, Yang J. Parathyroid carcinoma shown on ^{99m}Tc-sestamibi parathyroid SPECT/CT scan in a pediatric patient. Clin Nucl Med. 2020; 45(6): 480–2.
15. Castillo Cruz MN, Ramos CO. A case of an ectopic parathyroid adenoma with a concomitant ^{99m}Tc-sestamibi-avid papillary thyroid carcinoma. J Endocr Soc. 2021; 5(Suppl_1): A170–1.
16. Campi R, Pecoraro A, Serni S. Re: "Case of the Month" from the Specialist Centre for Kidney Cancer, Royal Free London Hospital, UK: ^{99m}Tc-sestamibi SPECT-CT to Differentiate Renal Cell Carcinoma from Benign Oncocytoma: The promise of value-oriented, cost-effective, shared decision-making for patients with localized renal masses: new imaging tools for a new diagnostic work-up. Eur Urol. 2022; 82(4): 443–4.
17. Wang R, Yu JQ, Schober JP, Standiford T, Bell S, Doss M, et al. Limited utility of quantitative thresholds on ^{99m}Tc-sestamibi SPECT/CT for distinguishing renal cell carcinoma from oncocytic renal masses. Eur Urol Open Sci. 2023; 60: S19–20.
18. Rowe SP, Murtazaliev S, Oldan JD, Kaufmann B, Khan A, Allaf ME, et al. Imaging of chromophobe renal cell carcinoma with ^{99m}Tc-sestamibi SPECT/CT: Considerations regarding risk stratification and histologic reclassification. Mol Imaging Biol. 2024; 26(5): 768–73.
19. Wang RS, Yu JQ, Schober J, Standiford T, Bell SH, Doss M, et al. Limited utility of quantitative thresholds on ^{99m}Tc-sestamibi SPECT/CT for distinguishing renal cell carcinoma from oncocytic renal masses. Urol Oncol. 2024; 42: S6–7.
20. Rajendran SG, Galgano SJ, Rais-Bahrami S. Editorial comment: Limited utility of quantitative thresholds on ^{99m}Tc-sestamibi single-photon emission computed tomography/computed tomography for distinguishing renal cell carcinoma from oncocytic renal masses. JU Open Plus. 2024; 2(9).